ELSEVIER

Triboelectrification-induced electroluminescent skin for real-time information recording at a record low pressure threshold of 0.125 kPa

Jiayu Li [a,b], Laipan Zhu [a,b,*], Zhiwei Zhang [a,b], Aochen Wang [c], Zhong Lin Wang [a,b,d,*], Longfei Wang [a,b,*], Dan Yang [e,*]

[a] Beijing Institute of Nanoenergy and Nanosystems, Chinese Academy of Sciences, Beijing 101400, China
[b] School of Nanoscience and Engineering, University of Chinese Academy of Sciences, Beijing 100049, PR China
[c] College of Electronic Information and Automation, Tianjin University of Science and Technology, Tianjin 300318, China
[d] Georgia Institute of Technology, Atlanta, GA 30332-0245, USA
[e] State Key Laboratory of Organic-Inorganic Composites, College of Materials Science and Engineering, Beijing University of Chemical Technology, Beijing 100029, China

The excitation of luminescent devices often requires complex structures with external power sources or intense mechanical stimuli. Herein, we report a novel triboelectrification-induced electroluminescent (TIEL) skin with a simple structure, which can much more efficiently convert weak mechanical aggitation into electrical and optical energy. The flexible TIEL skin utilizes a high smooth matrix PVP, and $Pb(Zr_xTi_{1-x}O_3)$ that enhances the dielectric property and the polarization of the skin, largely improving the triboelectric properties and luminescence intensity of the skin, respectively. The pressure threshold of TIEL skin breaks the record and reaches up to 0.125 kPa, which is ten-fold lower than the lowest pressure threshold of ZnS-based optic devices reported so far. It can not only trigger large-area luminescence, but also capture the dynamic motion of pen-tip like objects. Furthermore, TIEL skin successfully achieves remote real-time transmission and analysis of visualized information, which can precisely collect the optical information of handwriting and local single-point tracking, as well as obtain individual writing habits. This study shows a highly efficient way of self-powered visualized sensing, electronic signature, and anti-counterfeit information.

Keywords: Triboelectrification; Electroluminescence; ZnS:Cu; Phosphor; Flexible films

Introduction

Luminescence is a cold radiation, gradually becoming an integral element of human–machine information interfacing owing to its intuitiveness and visualization. It usually requires the induction of external stimuli, such as external electric field [1–3], piezoelectricity [4–6], mechanical force [7–9], magnetic field [10,11], light absorption [12,13], chemical reactions [5,14,15], or sound [16,17]. Among types of luminescence, electroluminescence (EL) could convert electrical information into human-readable optical information, widely applied in light sources/illumination displays [18,19], real-time visual sensing [20–23], wearable electronics [24–26], electronic skins [27,28], and electronic signatures/confidential information [28,29]. Nowadays, EL devices have evolved from rigid panels to flexible thin films, of which the sandwich-type design [30,31] is still difficult to achieve since it requires clamping of the electroluminescent layer and dielectric layer between two opaque and transparent electrodes. The complicated coplanar device structure increases not only cost but also requires high frequency and voltage drivers [18,32,33]. Additionally, the dielectric layer and the transparent electrode covering the electroluminescent layer weaken excitation light to some extent [22,34]. To solve these issues,

* Corresponding authors.
E-mail addresses: Zhu, L. (zhulaipan@binn.cas.cn), Wang, Z.L. (zhong.wang@mse.gatech.edu), Wang, L. (lfwang12@binn.cas.cn), Yang, D. (danyang@buct.edu.cn).

1369-7021/© 2024 Published by Elsevier Ltd. https://doi.org/10.1016/j.mattod.2024.06.010

triboelectrification-induced electroluminescent (TIEL) has attracted increasing interest in various appliactions [7,28,35–38]. Unlike mechanoluminescence (ML) which needs to be activated by strong mechanical motion at high pressure (up to MPa) or EL requiring an external power supply, TIEL may convert weak mechanical forces into light excitation with an ultra-low trigger threshold of pressure, advantageous in terms of low power consumption, portability, flexibility, and self-powered visual sensing.

Nevertheless, the established TIEL-based devices are limited in terms of complex device structures and low luminescence sensitivity. For example, most TIEL devices are fabricated by incorporating luminescent fillers into polymeric matrices, such as polydimethylsiloxane (PDMS), polymethyl methacrylate (PMMA), and polyurethane (PU). The large thickness caused by the traditional forming methods consume the emission of light inside the film, thereby weakening the luminescence intensity. In addition, traditional luminescent films usually possess non-smooth and sticky surfaces due to their excessively soft polymeric matrices, leading to high frictional resistance during sliding friction. As a result, the production of mechanical interactions requires large friction forces, resulting in an increased trigger threshold of pressure while affecting service life. To solve this, triboelectric layers have been coated on surfaces of luminescent films to obviate the direct horizontal sliding friction [35,36,39,40]. However, the complicated multilayer devices weaken the luminescence sensitivity and require high pressures to excite the TIEL. Therefore, developing flexible TIEL films combining high sensitivity with low triggering threshold and excellent brightness consisting of thin and simple structures are highly desirable.

Herein, a highly sensitive, self-powered, and flexible TIEL skin was fabricated by incorporating ZnS:Cu phosphorescent powder and $Pb(Zr_xTi_{1-x}O_3)$ (PZT) dielectric particles into the polyvinylpyrrolidone (PVP) matrix. The presence of PZT particles enhanced the dielectric properties and brightness of thin PVP/PZT/ZnS:Cu composite films. The as-obtained PVP/PZT/ZnS:Cu composite film exhibited surface smoothness with a thickness of 9.2 μm thanks to the superior film-forming properties, good biocompatibility, and high stability of PVP. PVP is a relatively tough and flexible material that avoids large deformations during friction and at the same time enables good contact with the slider. The superior surface properties endowed the TIEL skin with high sensitivity, as well as the ability to excite visible light at an extremely low-pressure threshold of 0.125 kPa, a value ten-fold lower than the lowest available threshold of ZnS-based optic devices reported so far. Moreover, the TIEL skin excited luminescence not only by slight friction of a large area slider but also by pen-like sliding on its surface. More importantly, the TIEL skin functioning as a visual sensing and optical information transfer not only achieved real-time optical imaging but also captured motion tracking by receiving real-time optical information. The collected optical information can then be synchronized and transmitted to the computer terminal to analyze individual writing habits of the hand writers for use in information anti-counterfeiting, smart sensor networks, and human–machine information interaction.

Results and discussion

The preparation, microstructure, and green light of PVP/PZT/ZnS:Cu composite film

As shown in Fig. 1**a, a** highly sensitive TIEL skin was developed that is capable of converting slight mechanical stimuli into optical signals readout in response to the object's motion position, trajectory, and handwriting habits. The detailed preparation procedure of PVP/PZT/ZnS:Cu composite film is provided in Fig. 1**b**. Briefly, ZnS:Cu phosphorescent particles were first homogeneously dispersed in the PVP solution. PZT powder was then introduced as a component and an appropriate amount of the mixture was taken and spin-coated on the polyvinyl chloride (PVC) substrate. After drying at room temperature, TIEL skin was obtained. The scanning electron microscopy (SEM) images of the composite film (Fig. 1**c** and **Figure S2**) showed uniformly dispersed ZnS:Cu phosphorescent particles with large particle sizes and relatively smooth surfaces. By comparison, the PZT particles with smaller sizes tended to aggregate in the PVP matrix. The elemental distribution of S, Cu, Zn, Ti, Pb, and Zr elements in PVP/PZT/ZnS:Cu composite film analyzed by energy dispersive spectrometer (EDS) proved the presence of ZnS:Cu and PZT particles (**Figure S2**). In X-ray diffraction (XRD) of PVP/PZT/ZnS:Cu composite film (Fig. 1**d**), the peaks at 2θ of 31.048° and 31.442° corresponded to the lattice planes (101) and (110) of PZT, respectively [41,42]. By comparison, ZnS:Cu exhibited two different individual phases due to the Cu-doped semiconductor aspect. The 2θ values of 26.995°, 30.603°, 47.587°, and 56.391° represented the four characteristic lattice planes (100), (101), (110), and (112) in Wurtzite-2H phase of ZnS, respectively [43–45]. The two characteristic lattice planes (111) and (200) at 28.602° and 33.096° demonstrated the formation of nantokite phase CuCl. The optical images of PVP/PZT/ZnS:Cu composite film are displayed in Fig. 1**e**. The cross-sectional SEM image in **Figure S3** revealed PVP/PZT/ZnS:Cu composite film displaying a thickness of 9.2 μm and a high surface smoothness, conducive to bright and sensitive TIEL. In addition, PVP/PZT/ZnS:Cu composite film possessed a photoluminescent function. As depicted by the fluorescence and absorption spectra (**Figure S4**), a sharp photoluminescence (PL) signal was observed at 497 nm for PVP/PZT/ZnS:Cu composite film [11,43], while the absorption peak was located at 362 nm. Such blue-shifting compared to the PL peak can be linked to the presence of ZnS:Cu component.

The TIEL properties were measured by subjecting PVP/PZT/ZnS:Cu composite film to horizontal sliding friction with triboelectric materials based on polytetrafluoroethylene (PTFE) or fluorinated ethylene propylene (FEP) adhering on the surface of an acrylic block used to make sliders with different sizes. As shown in **Video S1**, a bright green light emission was observed when the sliders were subjected to a direct relative horizontal sliding reciprocating motion with PVP/PZT/ZnS:Cu composite film. The corresponding luminescence spectrum in Fig. 1**f** displayed a luminescence peak of PVP/PZT/ZnS:Cu composite film at 512 nm, similar to PL spectra, demonstrating a green light region for both. PVP/PZT/ZnS:Cu composite film was not only triggered by a large area slider but also a pen-like slider allowing the observation of the luminous trajectory. Photographs of green light

Please cite this article in press as: J. Li et al., Materials Today (2024), https://doi.org/10.1016/j.mattod.2024.06.010

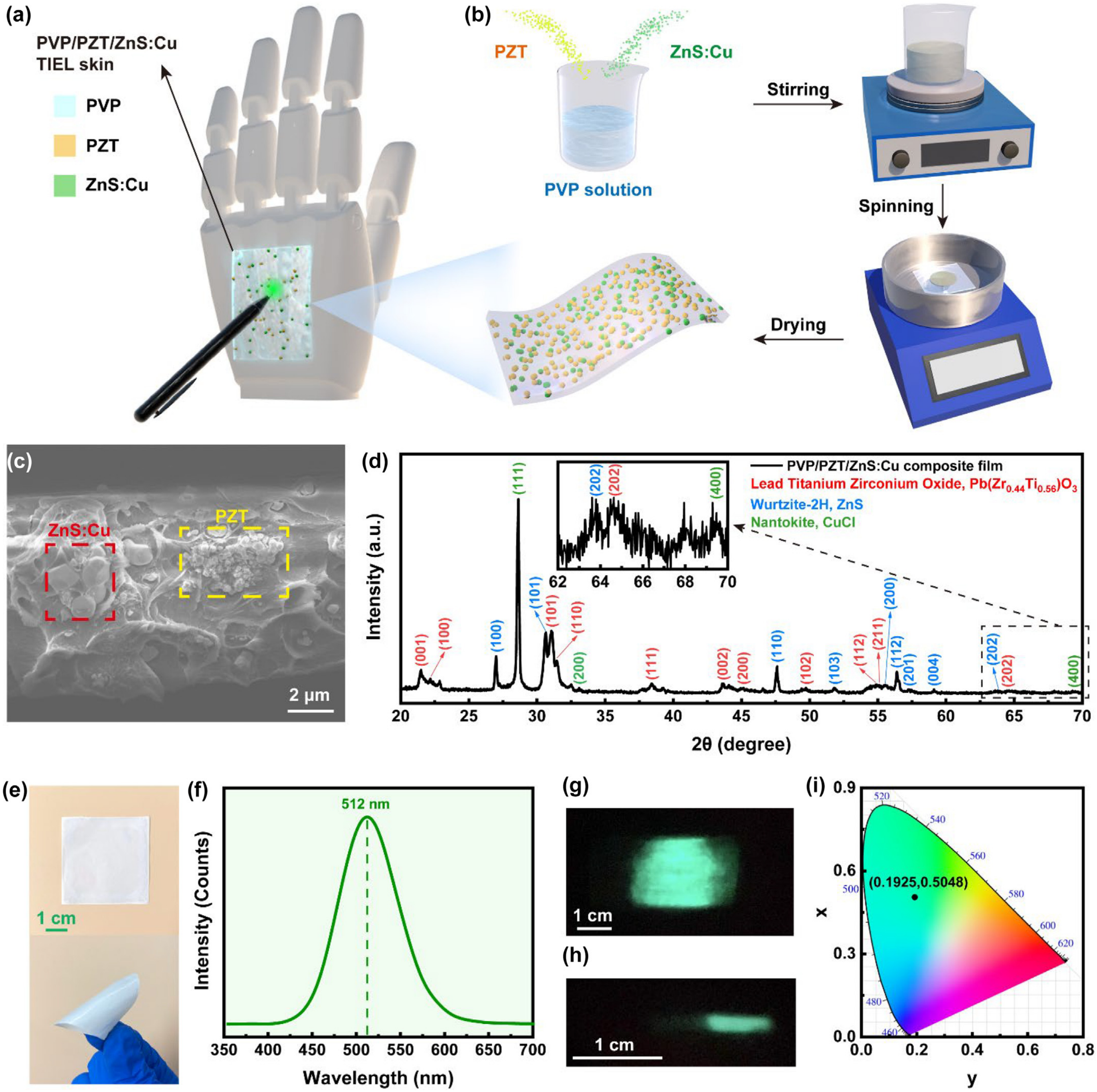

FIG. 1

Illustrations showing the preparation, microstructure, and green light of PVP/PZT/ZnS:Cu composite film. (a) TIEL schematic diagram. (b) Preparation procedure of PVP/PZT/ZnS:Cu composite film. (c) Cross-sectional SEM image of PVP/PZT/ZnS:Cu composite film. (d) XRD pattern of PVP/PZT/ZnS:Cu composite film. (e) Photographs of PVP/PZT/ZnS:Cu composite film. (f) Spectrum of TIEL. Luminescence induced by a slider with (g) a 2 cm × 2 cm square slider and (h) a 2 mm diameter circular slider. (i) CIE coordinates of TIEL.

acquired by horizontal sliding with a 2 cm × 2 cm square slider and a 2 mm diameter circular slider are presented in Fig. 1**g** and Fig. 1**h**, respectively. Comparison of the luminescence intensity of PVP/PZT/ZnS:Cu composite film with commercial LED shows that PVP/PZT/ZnS:Cu composite film was slightly brighter than a green LED driven by the power supply of 2 V, proving that it was sufficiently bright for practical use (**Figure S5**). It can even be able to observe a significant TIEL phenomena in daylight environments (**Video S2**). According to the Commission International de L'Eclairage (CIE) coordinates, the luminescence spectral data of TIEL were located in the green light region (Fig. 1**i**), consistent with the actual observation.

Please cite this article in press as: J. Li et al., Materials Today (2024), https://doi.org/10.1016/j.mattod.2024.06.010

RESEARCH (LIGHT BLUE)

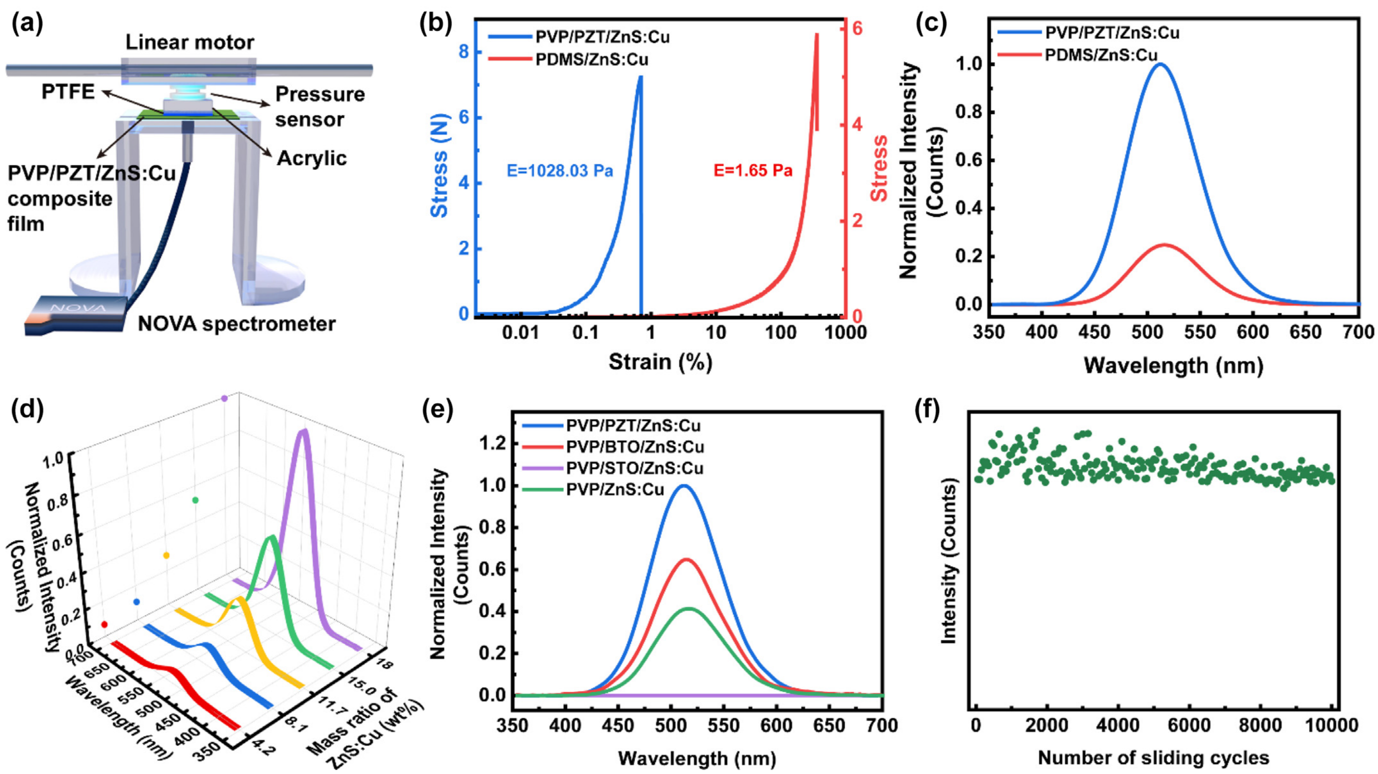

FIG. 2

The luminescence properties of PVP/PZT/ZnS:Cu composite film. (a) Schematic representation of TIEL testing device. (b) Stress–strain curves and (c) luminescence spectra of PVP/PZT/ZnS:Cu and PDMS/ZnS:Cu composite films. (d) Luminescence spectra of PVP/PZT/ZnS:Cu composite with different mass ratios of ZnS:Cu phosphor. (e) Comparison of luminescence properties of PVP/ZnS:Cu composite film and PVP composite films in the presence of added PZT, BTO, and STO. (f) The cyclic TIEL performance with 10000 sliding cycles.

The luminescence properties of PVP/PZT/ZnS:Cu composite film

The designed device for measurement of the luminescence properties of TIFL is depicted in Fig. 2**a**. In this setup, a holder was manufactured by cutting acrylic to act as a support for placing PVP/PZT/ZnS:Cu composite film. Subsequently, PVP/PZT/ZnS:Cu composite film fixed on the acrylic substrate surface was placed directly above the circular hole at the embedding place of the optical fiber probe. In this fashion, luminescence spectra excited from PVP/PZT/ZnS:Cu composite film could be captured along the motion trajectory of the slider by the optical fiber probe. Compared to the previous PDMS-based EL [46], the as-prepared PVP/PZT/ZnS:Cu composite film possessed a higher elastic modulus (Fig. 2**b and S6**), relatively smaller deformation, and ultra-high smoothness, eliminating the need of high pressure for light excitement. Our PVP/PZT/ZnS:Cu composite film with high surface smoothness imply more complete contact during sliding friction, which is favorable for reduction of the pressure threshold and increase in TIEL intensity (**Figure S7**). In **Figure S8**, the pressure threshold required for TIEL film-based PVP/PZT/ZnS:Cu composite film during the sliding process looked significantly reduced while the luminescence sensitivity greatly improved. Under the same pressure and horizontal sliding friction reciprocating motion frequency (Fig. 2**c**), the TIEL intensity of PVP/PZT/ZnS:Cu composite film was estimated to be about five-fold higher than that of PDMS/ZnS:Cu composite film, showing significantly superior luminescence performances.

In addition, the TIEL intensity obviously enhanced as a function of the content of ZnS:Cu phosphor particles (Fig. 2**d**). In the presence of added PZT, the TIEL intensity of PVP/PZT/ZnS:Cu composite film was about 2.5-fold higher than that of PVP/ZnS:Cu composite film (Fig. 2**e**). The importance of PZT was further demonstrated by adding barium titanate (BTO) and strontium titanate (STO) dielectric filler into the PVP matrix for comparison. As displayed in Fig. 2**e**, no luminescence was detected for PVP/STO/ZnS:Cu composite film. Also, despite observing TIEL emission for PVP/BTO/ZnS:Cu composite film, the TIEL intensity was distinctly weaker than that of PVP/PZT/ZnS:Cu composite film. Several of the above additions are chalcogenide-type piezoelectric ceramics. However, they did not exhibit similar properties in the composite films. Hence, the differences in luminescence intensities between the above composite films can exclude the effects of piezoelectric polarization as well as ferroelectric polarization. Otherwise, the chalcogenide-type piezoelectric ceramics show high dielectric properties. The corresponding dielectric permittivity of PVP/ZnS:Cu composite films with various dielectric fillers are shown in **Figure S9**. PVP/PZT/ZnS:Cu composite film exhibited the highest dielectric permittivity, followed by PVP/BTO/ZnS:Cu composite film, while PVP/ZnS:Cu without any dielectric additives depicted the lowest value. Consequently, the main reason for the high TIEL intensity of PVP/PZT/ZnS:Cu composite film was linked to enhanced dielectric permittivity of PZT.

Please cite this article in press as: J. Li et al., Materials Today (2024), https://doi.org/10.1016/j.mattod.2024.06.010

As for the repeatability and stability of the TIEL, the cyclic characteristic is measured when the slider repeatedly slides against PVP/PZT/ZnS:Cu composite film in a reciprocating way (cyclic frequency: 2 Hz; contact pressure: 1.25 kPa). The peak luminescence intensity of each 50 cycles is recorded and as shown in Fig. 2**f**. After 10,000 cycles, the luminescence only dropped slightly, demonstrating good stability and repeatability. Also, we measured the tolerance of TIEL skin to humidity. As shown in **Figure S10**, it was observed that the luminescence intensity of TIEL skin gradually decreased as the humidity gradually increased. When the humidity reaches 70 %, the TIEL skin will bend due to excessive moisture absorption. As a result, our TIEL skin exhibits a certain sensitivity to humidity. However, TIEL skin will function properly as long as the humidity is below 70 %.

Mechanism of TIEL based on PVP/PZT/ZnS:Cu composite film

According to the triboelectric series [47], PTFE can be used as an excellent negative triboelectric material owing to its surface that can be negatively charged. Here, PTFE was used as a triboelectric slider to form horizontal sliding friction with PVP/PZT/ZnS:Cu composite film. Also, the positive PVP matrix would result in a PVP/PZT/ZnS:Cu composite film surface carrying positive charges. The detailed mechanism analyses of the TIEL based on PVP/PZT/ZnS:Cu composite film (Fig. 3**a** (I)) and PVP/ZnS:Cu composite film (Fig. 3**a** (II)) during triboelectric charging process rubbed against PTFE are illustrated in Fig. 3**a**. Based on the conservation of electric charge and the basic principle of triboelectrification, both PTFE film and TIEL composite film would have equal and opposite charges on their surfaces under an electric field. The electric field between both surfaces would continuously change due to the sliding reciprocating motion of the PTFE slider on PVP/PZT/ZnS:Cu composite film surface. The variation in the electric field increased the driving frequency of TIEL device, which enhanced the electron-hole recombination rate and gained an EL on TIEL. After the introduction of PZT, the enhanced dielectric permittivity of PVP/PZT/ZnS:Cu composite film exhibited a more concentrated electric field on ZnS:Cu particles in the matrix than PVP/ZnS:Cu composite film, thereby enhancing the polarization and increasing the TIEL. In other words, the changing electric field around ZnS:Cu particles induced equal and opposite charges at its upper and lower sides. A local electric field was then formed between the oppositely polarized charges on ZnS:Cu particles, resulting in a tilted energy band of ZnS. Meanwhile, the electrons trapped on the shallow donor level became lightly detrapped to yield free electrons in the conduction band. Eventually, the released electrons combine with the holes on the deep acceptor level of the impurity state of Cu via a nonradiative recombination, resulting in the ZnS:Cu particles emitting green light (Fig. 3**b**) [45,48,49].

The potential distribution of the PVP/PZT/ZnS:Cu composite film during the horizontal sliding reciprocating motion with PTFE film is presented in Fig. 3**c**. Since PTFE continued to slide reciprocally on PVP/PZT/ZnS:Cu composite film surface, the charges in surface of PVP/PZT/ZnS:Cu composite film became extensively positively charged with a total number of charges equal to negative charges on PTFE surface. The smaller area resulted in larger surface tribocharge density in PTFE than in PVP/PZT/ZnS:Cu composite film, leading to a stronger effect of the surface tribocharges in PTFE on the interior property of TIEL than own surface charge of PVP/PZT/ZnS:Cu composite film. Additionally, the luminescence ranges of TIEL was slightly larger than the contact area between PTFE and PVP/PZT/ZnS:Cu composite film during the experiments. The potential distributions on PVP/PZT/ZnS:Cu composite film surface with different PTFE slider areas are displayed in Fig. 3**d–e**. The strongest potential on TIEL surface was concentrated on the contact part with the slider, regardless of the shape and area of the slider. Moreover, a decay region progressively varying around the contact range was noticed due to no abrupt change in surface potential but coherent change was induced.

The properties of TIEL were further explored by numerical simulations (**Table S1** and **Figure S1**). Fig. 3**f** illustrates the influence of the surface tribocharge density of PTFE on electric potential of PVP/PZT/ZnS:Cu composite film under sliding motion. As expected, the PTFE materials with higher surface tribocharge density induced a higher surface potential of PVP/PZT/ZnS:Cu composite film, resulting in brighter emitted visible light. Moreover, bright green light can be easily detected on both large-area sliders and small-area pen-like sliders. The impacts of PTFE sliders with side lengths ranging from 0.0625 to 2 cm on surface potential of PVP/PZT/ZnS:Cu composite film are displayed in Fig. 3**g**. As the area of the PTFE sliders decreased, the change in the surface potential of PVP/PZT/ZnS:Cu composite film enlarged due to the smaller area of PTFE slider that resulted in more concentrated tribocharges and greater effect of leakage electric field on PVP/PZT/ZnS:Cu composite film. The theoretical calculations based on electric potential along the thickness of PVP/PZT/ZnS:Cu composite film are provided in Fig. 3**h**, where (I) corresponds to a larger area PTFE slider and (II) represents a smaller area PTFE slider. For a larger area of PTFE slider, the trend of the electric potential of PVP/PZT/ZnS:Cu composite film looked close to a straight line. In other words, the potential decreased uniformly along the thickness direction. By contrast, the decline in area of PTFE slider to a certain degree resulted in the curvy trend of the electric potential of PVP/PZT/ZnS:Cu composite film with rapid change in potential slow variation until reaching zero, different from uniform change along the thickness direction.

Optimization of TIEL performance based on PVP/PZT/ZnS:Cu composite film

The dielectric permittivity of PVP/PZT/ZnS:Cu composite film with different contents of PZT are given in Fig. 4**a**. Obviously, the dielectric permittivity of PVP/PZT/ZnS:Cu composite film increased with the addition of PZT to reach a maximum value of 1.33 (1 kHz) at 10.8 wt%. By comparison, PVP/ZnS:Cu composite film without PZT exhibited the lowest dielectric permittivity of about 1.13 (1 kHz). According to previous work [50], when high-dielectric-permittivity materials are used in electroluminescent devices, it is possible to concentrate the strong electric field on ZnS:Cu particles, which have relatively low dielectric-permittivity, and thus improve the luminescence efficiency. However, the dielectric permittivity of PVP/PZT/ZnS:Cu composite film with PZT content of 13.9 wt% decreased to 1.17 (1 kHz) due to the large amount of PZT that resulted in numerous aggregates in the PVP matrix, which weakened the interfacial polariza-

Please cite this article in press as: J. Li et al., Materials Today (2024), https://doi.org/10.1016/j.mattod.2024.06.010

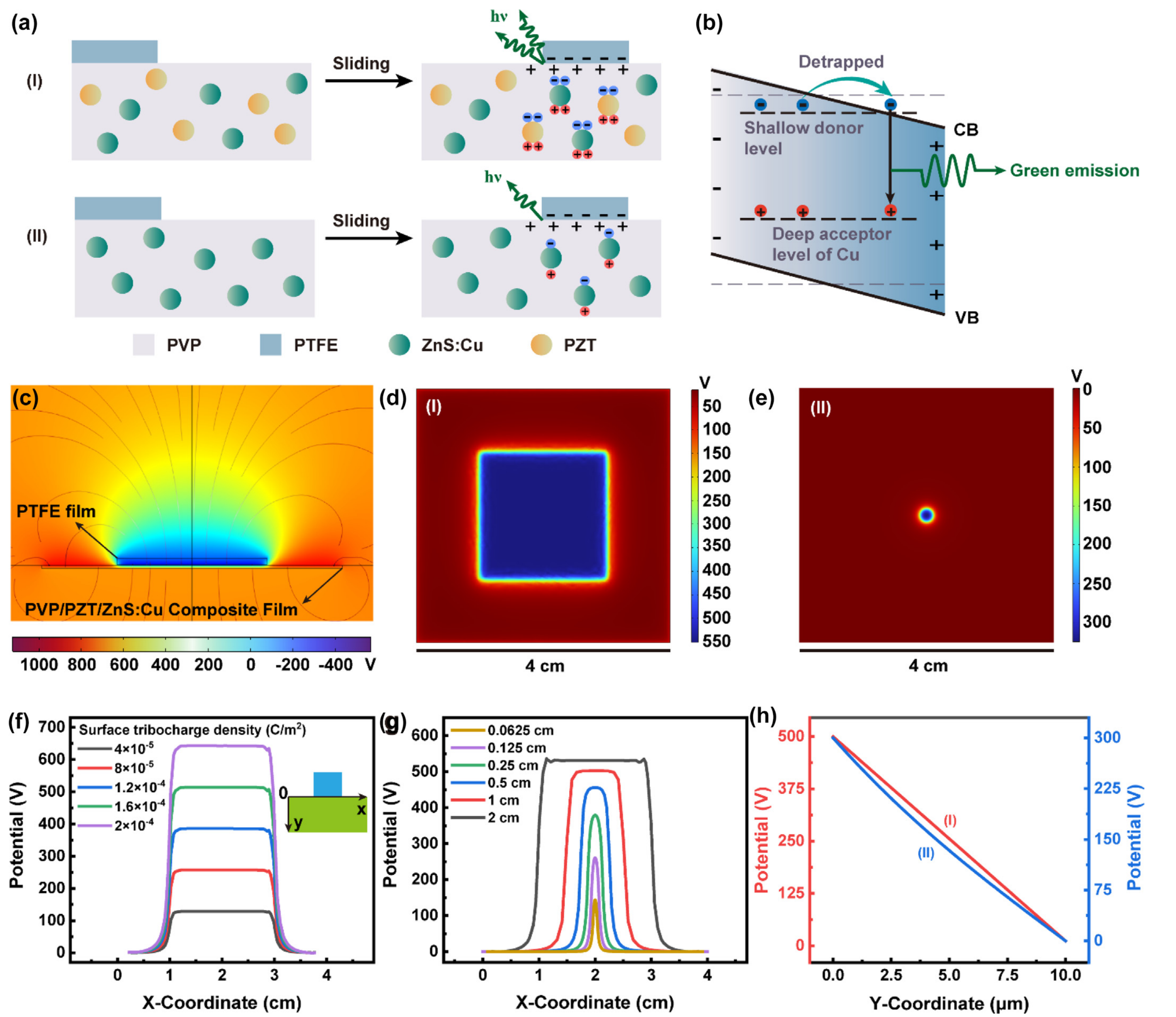

FIG. 3

Mechanism of TIEL based on PVP/PZT/ZnS:Cu composite film. (a) Schematic diagram of charge distribution between PTFE triboelectric materials and (I) PVP/PZT/ZnS:Cu composite film and (II) PVP/ZnS:Cu composite film. (b) Energy band diagram describing the TIEL mechanism of PVP/PZT/ZnS:Cu composite film. (c) Simulated electric field between PTFE and PVP/PZT/ZnS:Cu composite film. (d–e) Electric potential distribution of PVP/PZT/ZnS:Cu composite contact with (I) a 2 cm × 2 cm square slider and (II) a 2 mm diameter circular slider. (f) The effect of surface tribocharge density of PTFE on electric potential of PVP/PZT/ZnS:Cu composite film. (g) The impact of length of square sliders on electric potential of PVP/PZT/ZnS:Cu composite film. (h) The trend of electric potential along the thickness of PVP/PZT/ZnS:Cu composite film.

tion (Maxwell – Wagner – Sillars polarization) and lowered the dielectric permittivity [51–53]. The TIEL spectra of PVP/PZT/ZnS:Cu composite films with different contents of PZT were further measured. As depicted in Fig. 4**b**, the TIEL intensity of PVP/PZT/ZnS:Cu composite films increased gradually as a function of PZT content from 0 to 10.8 wt%, with maximum luminescence intensity obtained at 10.8 wt%. Nevertheless, no luminescence was observed at a PZT content of 13.9 wt%, which is consistent with the changes of dielectric permittivity of the above films. Thus, certain content of PZT can improve the dielectric permittivity of PVP/PZT/ZnS:Cu composite film and strengthen its TIEL intensity, while more content of PZT did not only decrease the dielectric permittivity of PVP/PZT/ZnS:Cu composite film but also blocked the release of the emitted light from ZnS:Cu phosphor particles inside PVP/PZT/ZnS:Cu composite film. Moreover, the luminescence properties of PVP/PZT/ZnS:Cu composite film under mechanical stimuli with different frequencies were also investigated. As the relative horizontal sliding reciprocal motion frequency of the PTFE slider slowly rose from 0.5 to 3 Hz, the TIEL intensity in the luminescence spec-

Please cite this article in press as: J. Li et al., Materials Today (2024), https://doi.org/10.1016/j.mattod.2024.06.010

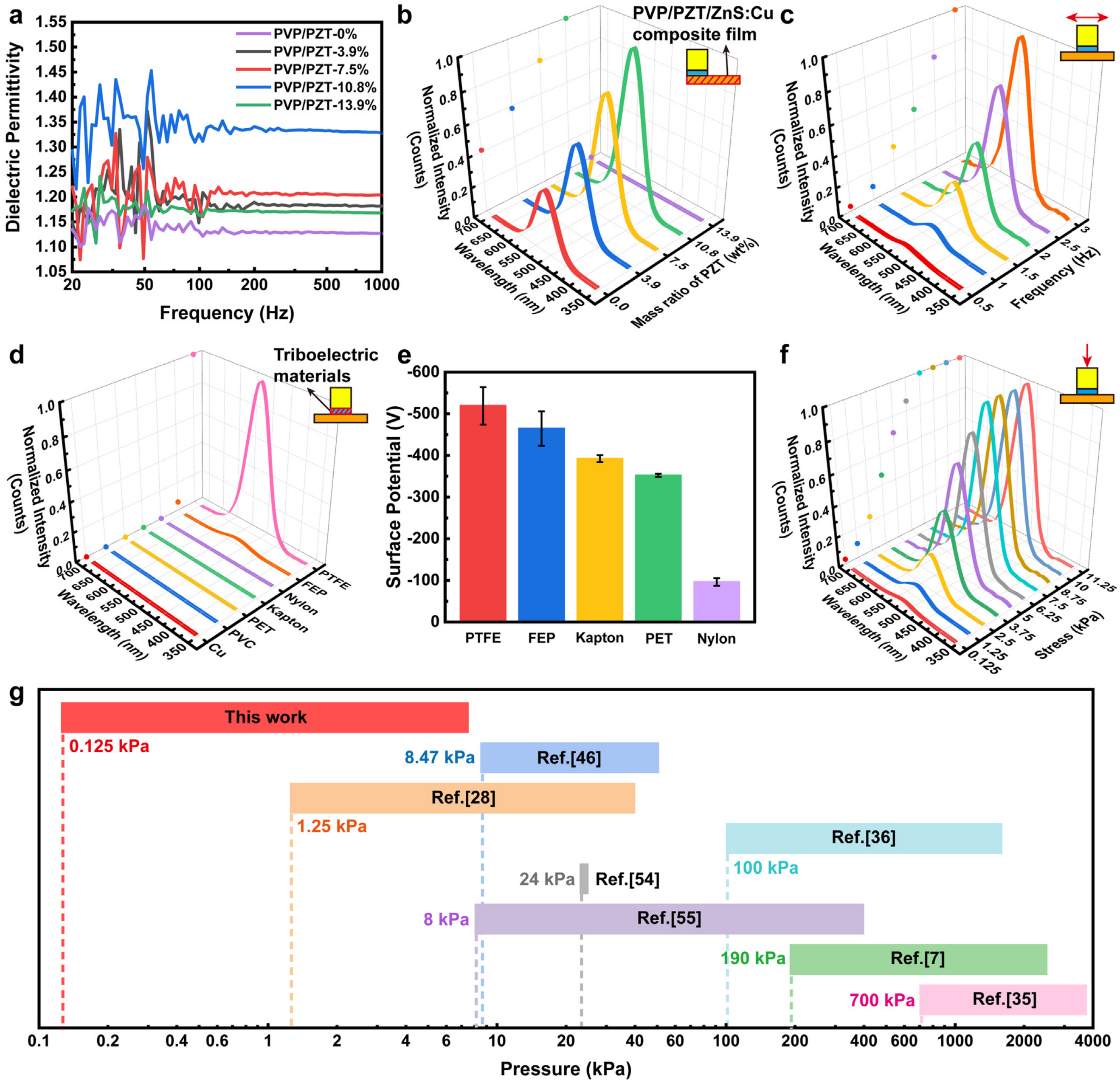

FIG. 4

Optimization of TIEL performance based on PVP/PZT/ZnS:Cu composite film. (a) The relative permittivity of PVP/PZT/ZnS:Cu composite film with different different mass ratios of PZT. (b–d) The luminescence intensity of PVP/PZT/ZnS:Cu composite film with different mass ratios of PZT, sliding frequencies, and triboelectric material. (e) The surface potential values of PVP/PZT/ZnS:Cu composite film rub with different triboelectric materials during sliding. (f) The luminescence intensity of PVP/PZT/ZnS:Cu composite film under different stresses. (g) Comparison of a bar chart of the pressure threshold values between this work and other published works.

trum of PVP/PZT/ZnS:Cu composite film gradually increased (Fig. 4**c**). The accelerated motion frequency meant an increase in number of sliding over a certain local area per unit of time. Thus, ZnS:Cu phosphor particles in PVP/PZT/ZnS:Cu composite film were excited more times per unit time to emit brighter visible light.

In addition to PTFE, various typical triboelectric materials for TIEL, such as FEP, Nylon, Kapton, polyethylene terephthalate (PET), PVC, and Cu were explored (Fig. 4**d**). Only PTFE and FEP triggered green light emissions, of which the TIEL intensity based on the PTFE reaching a 24.5-fold higher than that of FEP under the same triggering conditions. This phenomenon was clarified by measuring the surface potential of these triboelectric materials using PVP/PZT/ZnS:Cu composite film by horizontal sliding reciprocal motion. In this case, the surface potential value of the triboelectric materials before friction was considered to be zero, while those after multiple measurements were averaged to obtain Fig. 4**e** and **Figure S11**. The surface potentials of PTFE,

Please cite this article in press as: J. Li et al., Materials Today (2024), https://doi.org/10.1016/j.mattod.2024.06.010

FEP, Kapton, PET, and Nylon showed a decreasing order. The surface potential of PTFE reached the largest value at −519 V, followed by FEP at −464.5 V. Hence, the surface potential threshold of EL in PVP/PZT/ZnS:Cu composite film ranged between those of FEP and Kapton (−464.5 V to −392.5 V). Therefore, both FEP and PTFE with surface potential above the surface potential threshold were able to obtain TIEL with PVP/PZT/ZnS:Cu composite film through sliding. Generally, not much difference in the surface potential was recorded between PTFE and FEP, but their TIEL intensities contrasted sharply. It can be attributed to the higher elastic modulus of PTFE (**Figure S12**), leading to more effective contact between PTFE and PVP/PZT/ZnS:Cu composite film during horizontal sliding friction. Furthermore, the pressure applied to the PTFE slider in the vertical direction significantly affected the TIEL intensity during the sliding process. As shown in Fig. 4**f**, the TIEL intensity rose linearly as a function of pressure to reach saturation at a pressure of 3 N, equivalent to 7.5 kPa. As for PVP/PZT/ZnS:Cu composite film, the emission of green light was observed at a minimum vertically applied pressure of 0.05 N, equivalent to 0.125 kPa. The latter value was ten-fold lower than the lowest reported trigger pressure of TIEL (Fig. 4**g**). The low threshold obtained in the present work in the bar chart of Fig. 4**g** [7,28,35,36,46,54,55] can be attributed to the excellent triboelectrification performance and superior surface smoothness of PVP/PZT/ZnS:Cu composite film.

Applications of TIEL skin in real-time information recording and imaging

Motivated by the rapid development of the Internet of Things, human–machine interface applications and wearable skins

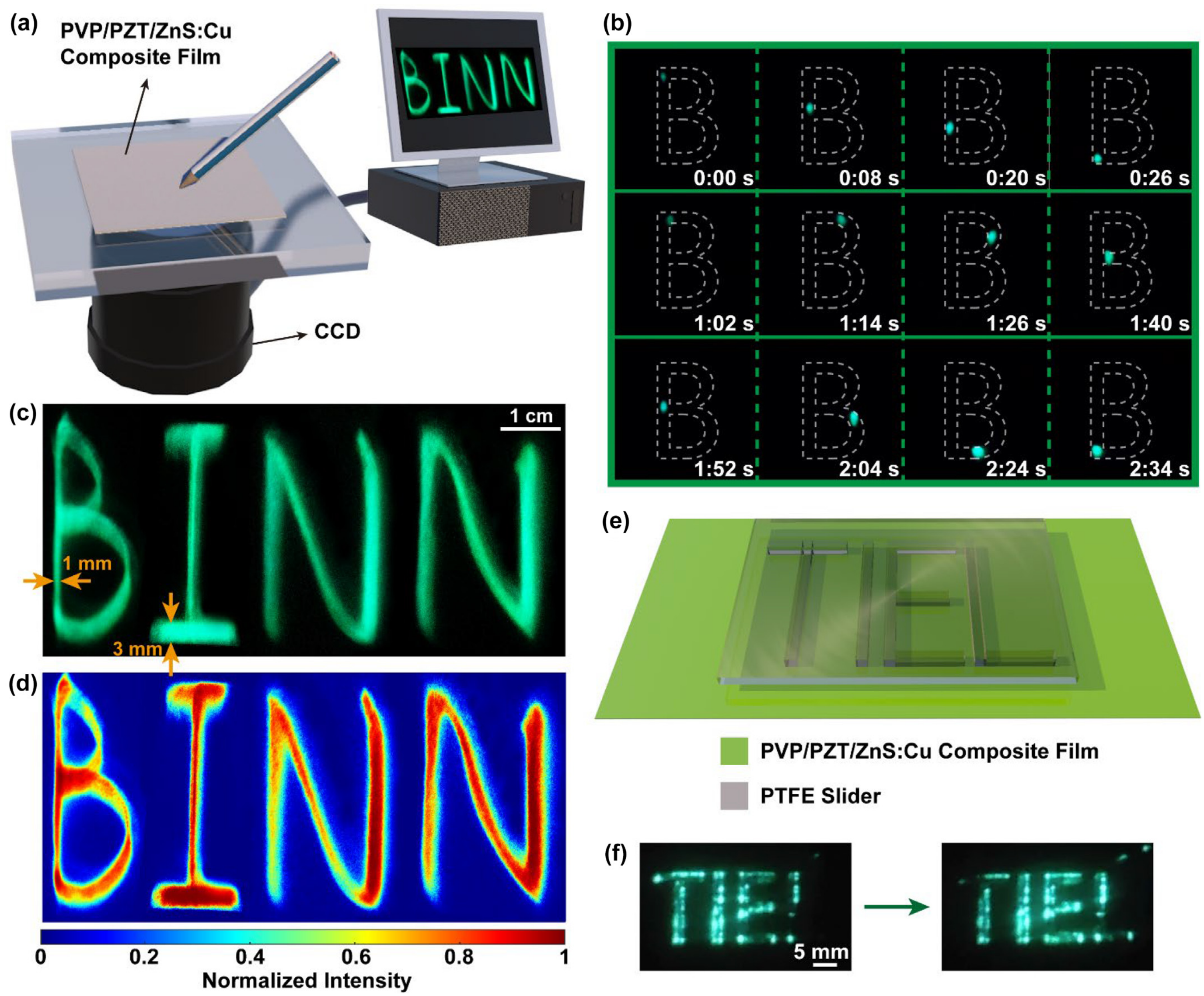

FIG. 5

Applications of TIEL skin in real-time information recording and imaging. (a) Demonstration of the image acquisition system. (b) Images captured by a digital camera in consecutive frames during handwriting. (c–d) Luminescence image and its corresponding mapping of normalized intensity induced by a pen-like object. (e–f) Schematic TIEL and its luminescence image photographs excited by a patterned slider.

Please cite this article in press as: J. Li et al., Materials Today (2024), https://doi.org/10.1016/j.mattod.2024.06.010

[56–63], TIEL films with low-pressure thresholds can be excited by weak mechanical interactions to generate optical outputs at the moment of excitation. If optical information can be transmitted, received, and analyzed, it can effectively be utilized for cloud data exchange, making it more attractive for sensing and artificial intelligence applications. In the application of real-time information recording, lowering the pressure threshold indicates that the monitoring range of TIEL film is extended. It means that a much weaker external stimulus can cause TIEL film to emit light, which can be used in special situations, such as monitoring the movement of extremely light objects, or even for people who are sick or have insufficient strength. In addition, when we use TIEL films for real-time information recording in the field of human–machine interaction, the mechanical movements of robots are in most cases unstable and unevenness, which can be captured by TIEL films with a low pressure threshold.

Inspired by this, an image acquisition system was designed (Fig. 5**a**), in which PVP/PZT/ZnS:Cu composite film was placed on top of a transparent platform, while a charge-coupled device (CCD) was placed on the back of the transparent substrate. Fig. 1**f**-g suggested that high sensitivity of PVP/PZT/ZnS:Cu composite film was not only trigger by large-area sliders but also by small-area sliders. As depicted in **Videos S3** and **S4**, a pen-like object with soft PTFE heads was used to realize optical information transmission by handwriting on PVP/PZT/ZnS:Cu composite film surface. The decomposition diagrams of the handwritten letter “B” collecting the real-time position of the visualized handwritten information are displayed in Fig. 5**b**. Here, successive real-time images were recorded at different time points. The varying degrees of contact at each intercept point during the handwriting process resulted in different intensities or luminous areas of each point of the TIEL. By combining and superimposing these screenshots together, an overall tracing of the letter “B” was formed. By taking time-lapse photos with the digital camera followed by computer acquisition via Wi-Fi resulted in a complete recording of the handwritten message “BINN” (Fig. 5**c**, **Video S4**). Depending on the uneven force applied to the pen by the hand, the finest part of the image was estimated to be 1 mm while the thickest was 3 mm. Also, the overall handwriting looked delicate, bright, and clear. In Fig. 5**d**, the images were processed through MATLAB software to obtain the corresponding mapping of the normalized TIEL intensity of the handwritten message. Through mapping, observing the writing habits of the handwriting was possible, including lighter strokes at the beginning, harder strokes at the corner of the front, and heavier strokes at the end, useful for electronic signatures and anti-counterfeit messages to protect the information. In this way, CCD can collect optical information via computer acquisition to translate light information in real-time into analysis data. In addition, the PTFE slider was designed to convey the desired message by sliding horizontally and reciprocally on PVP/PZT/ZnS:Cu composite film surface (Fig. 5**e**), and a clear luminescent image of “TIEL” was captured at the remote computer corresponding to the pattern of the slider sliding from left to right (Fig. 5**f**). Overall, PVP/PZT/ZnS:Cu TIEL skin resulted in an efficient, real-time, and secure human–machine information interaction system via optical information long-distance transmission, capable of simultaneously achieving single-point dynamic position recording and complete optical information trajectory recording. It also allowed analysis and interpretation of individual writing behavior, including writing speed and exertion habits, enabling secure electronic signature and information transfer.

Conclusion

We have developed a highly sensitive, smooth, and flexible TIEL skin by incorporating ZnS:Cu phosphorescent powder and PZT dielectric particles into the PVP matrix, which can efficiently convert the weak mechanical interaction into electrical and optical energy. Owing to the surface smoothness of the skin, and the presence of PZT particles that can enhance the dielectric properties and the polarization of skin, the triboelectric properties and luminescence intensity of TIEL skin are largely improved. The mechanism of TIEL is further explored by theoretical simulations, which suggests that the surface potential and surface charge density also have an important influence on triboelectrification and luminescence. As expected, the TIEL exhibits an extremely low pressure threshold of 0.125 kPa, which is tenfold lower than the lowest pressure threshold reported so far. It can not only trigger large-area luminescence but also capture the dynamic motion of pen-like objects. More importantly, the visual sensing and optical information transmission capabilities of TIEL skin not only enable real-time optical imaging, but also capture motion tracking by receiving real-time optical information. These features look promising for application in security anti-counterfeiting, electronic commerce, and human–machine information interaction by analyzing the optical information.

Experimental section

Materials. ZnS:Cu (D502CT, 1 μm) was supplied by Shanghai Keyan Phosphor Technology Co., Ltd. China. PVP was purchased from Aladdin. PZT (100 nm) was provided by Qi Jin New Material, Ltd. China. The PTFE thin film was received from Chukoh Chemical Industries, Ltd. China. The FEP, PET, Kapton, Nylon, and Cu were all commercially available film tapes.

Synthesis of PVP/PZT/ZnS:Cu Composite Films. The process consisted of adding 0.4 g PVP to 3 mL ethanol followed by stirring until complete dissolution of the powder. An appropriate amount of PZT powder was then weighed and placed in the PVP solution followed by stirring thoroughly and ultrasonic treatment for 30 min to uniformly disperse PZT powder in PVP solution. An appropriate amount of ZnS: Cu powder was then added to the above mixture and spin-coated onto 4 cm × 4 cm PVC substrates obtained by cutting. The platforms were then left in a ventilated area at room temperature until complete drying and final peeling of the film.

Preparation of Measuring Device. A holder was manufactured by cutting acrylic to act as a support for placing PVP/PZT/ZnS:Cu composite film. The circular hole with a diameter of 7 mm in the holder was used for embedding the optical fiber probe of the luminescence spectrometer. A linear motor was applied to control the movement of the slider, and a pressure sensor was placed between the linear motor and the slider to monitor the corresponding pressure in real-time. The optical

Please cite this article in press as: J. Li et al., Materials Today (2024), https://doi.org/10.1016/j.mattod.2024.06.010

fiber probe was fixed immovably with a clamp during the horizontal sliding reciprocating motion of the slider.

Characterization of PVP/PZT/ZnS:Cu Composite Films. The optic fiber was used to collect the light emission to a spectrometer (NOVA). The surface potentials of PVP/PZT/ZnS:Cu composite films were recorded by an electrostatic voltmeter (Trek MODEL 347). Microscopic images of the composite films and elemental mappings were viewed by scanning electron microscopy (SEM, SU8020, Hitachi). The structure was determined by X-ray diffraction (XRD, Xpert3 Powder). The PL spectra of the composite films were recorded by Fluorescence and Phosphorescence Lifetime Spectrometer (PL, EI/FLS980-S2S2-stm). The absorption spectra were measured by a UV–Vis-NIR Spectrophotometer (Shimadzu/UV3600).

CRediT authorship contribution statement

Jiayu Li: Writing – original draft, Investigation, Data curation. **Laipan Zhu:** Writing – review & editing, Supervision, Project administration. **Zhiwei Zhang:** Investigation, Data curation. **Aochen Wang:** Investigation, Data curation. **Zhong Lin Wang:** Writing – review & editing, Supervision, Project administration. **Longfei Wang:** Writing – review & editing, Supervision, Project administration. **Dan Yang:** Writing – review & editing, Supervision, Project administration.

Data availability

Data will be made available on request.

Declaration of competing interest

The authors declare that they have no known competing financial interests or personal relationships that could have appeared to influence the work reported in this paper.

Acknowledgements

The National Natural Science Foundation of China (Grant 52202162) and the National Key R&D Project from the Minister of Science and Technology (2021YFA1201601).

Appendix A. Supplementary material

Supplementary data to this article can be found online at https://doi.org/10.1016/j.mattod.2024.06.010.

References

[1] A. Fakharuddin et al., Nat. Electron. 5 (2022) 203.
[2] L. Zhang et al., Adv. Mater. 35 (2023) 2302059.
[3] J. Zhang et al., Adv. Mater. 34 (2022) 2200334.
[4] P. Xia et al., Adv. Energy Mater. 13 (2023) 2301332.
[5] J.I. Lee et al., Adv. Mater. 33 (2021) 2100321.
[6] Y. Zhao et al., Adv. Funct. Mater. 31 (2021) 2010265.
[7] B. Zhou et al., Nano-Micro Lett. 15 (2023) 72.
[8] T. Zheng et al., Adv. Mater. 35 (2023) 2304140.
[9] B. Hou et al., Nat. Electron. 5 (2022) 682–693.
[10] S.W. Lee et al., Nat. Commun. 11 (2020) 6072.
[11] M.C. Wong et al., Adv. Mater. 27 (2015) 4488.
[12] G. Lee et al., Adv. Mater. 32 (2020) e1907477.
[13] H. Yang et al., Adv. Mater. 35 (2023) 2301300.
[14] S. Lee et al., Adv. Mater. 33 (2021) 2005456.
[15] M. Yang et al., Chem. Soc. Rev. 49 (2020) 6800.
[16] S. Cho et al., Adv. Sci. 8 (2020) 2001647.
[17] J.S. Kim et al., Nano Energy 59 (2019) 773.
[18] F. Stauffer, K. Tybrandt, Adv. Mater. 28 (2016) 7200.
[19] Y. Zhou et al., Lett. 1 (2019) 511.
[20] X. Xu et al., Adv. Mater. 29 (2017) 1703552.
[21] L. Su et al., Adv. Sci. 6 (2019) 1901980.
[22] W. Jin et al., Adv. Funct. Mater. 31 (2021) 2010492.
[23] C. Qu et al., Nano Energy 104 (2022) 107965.
[24] H. Mi et al., Mater. Interfaces 13 (2021) 11260.
[25] X. Shi et al., Nature 591 (2021) 240.
[26] H.J. Park et al., Mater. Interfaces 11 (2019) 5200.
[27] C. Larson et al., Science 351 (2016) 1071.
[28] C. Jia et al., Adv. Funct. Mater. 32 (2022) 2201292.
[29] Q. Cheng et al., J. Mater. Chem. C 7 (2019) 4567.
[30] H. Dinh Xuan et al., Adv. Mater. 33 (2021) 2008849.
[31] Y. Zuo et al., Adv. Funct. Mater. 30 (2020) 2005200.
[32] C.H. Yang et al., Adv. Mater. 28 (2016) 4480.
[33] B. You et al., Mater. Interfaces 9 (2017) 5486.
[34] X. Liu et al., Adv. Funct. Mater. 32 (2022) 2106411.
[35] X.Y. Wei et al., Adv. Mater. 28 (2016) 6656.
[36] L. Su et al., Nano Energy 79 (2021) 105431.
[37] L. Su et al., Mater. Horiz. 10 (2023) 2445.
[38] L. Su, H. Wang, Y. Zi, J. Phys. Mater. 4 (2021) 042001.
[39] X.J. Zhao et al., Nano Energy 75 (2020) 104823.
[40] X.Y. Wei et al., Nano Energy 61 (2019) 158.
[41] K. Thanigai Arul, M. Ramanjaneyulu, M.S. Ramachandra Rao, Curr. Appl. Phys. 19 (2019) 375.
[42] K. Thanigai Arul, M.S. Ramachandra Rao, J. Phys. Chem. Solids. 146 (2020) 109371.
[43] H. You et al., Mater. Lett. 219 (2018) 155.
[44] M. PourhosseiniAsl et al., Adv. Mater. Interfaces 10 (2023) 2202332.
[45] X.D. Wang et al., Adv. Mater. 27 (2015) 2324.
[46] J. Li et al., Mater. Interfaces 14 (2022) 4775.
[47] H. Zou et al., Nat. Commun. 10 (2019) 1427.
[48] J.F. Wager, P.D. Keir, Annu. Rev. Mater. Sci. 27 (1997) 223.
[49] M. Dür et al., J. Appl. Phys. 83 (1998) 3176.
[50] H. Lee et al., Mater. Interfaces 15 (2023) 16299.
[51] U. Abaci, H.Y. Guney, M. Yilmazoglu, Polym. Polym. Compos. 29 (2021) S565.
[52] U.H. Choi et al., Mater. Interfaces 8 (2016) 3215.
[53] M. Kumar, S.S. Sekhon, Eur. Polym. J. 38 (2002) 1297.
[54] Y. Wang et al., Mater. Interfaces 11 (2019) 13796.
[55] X.Y. Wei et al., Adv. Mater. Interfaces 5 (2018) 1701063.
[56] M. Zhu et al., Angew. Chem. Inter. Ed. 61 (2022) e202200226.
[57] J. Cai, M. Du, Z. Li, Adv. Mater. Technol. 7 (2022) 2101182.
[58] X. Lv et al., Adv. Fiber Mater. 5 (2023) 401.
[59] M. Zhu et al., Angew. Chem. Inter. Ed. 61 (2022) e202208949.
[60] J. Li et al., Adv. Funct. Mater. 33 (2023) 2303249.
[61] P. Basset, S.P. Beeby, C. Bowen, et al., APL Materials. 10 (2022) 109201.
[62] Y. Chen et al., Exploration 2 (1) (2022) 20210112.
[63] Z. Dai et al., Exploration (2024) 20230046.

Please cite this article in press as: J. Li et al., Materials Today (2024), https://doi.org/10.1016/j.mattod.2024.06.010